Deep Learning based Nuclei Segmentation in Histopathological Images:
A perspective on Image Normalization

by

Kishankumar Vaishnani
202011004

A Thesis Submitted in Partial Fulfilment of the Requirements for the Degree of

MASTER OF TECHNOLOGY
in
INFORMATION AND COMMUNICATION TECHNOLOGY
to

DHIRUBHAI AMBANI INSTITUTE OF INFORMATION AND COMMUNICATION TECHNOLOGY

May, 2022

Declaration

I hereby declare that

i) the thesis comprises of my original work towards the degree of Master of Technology in Information and Communication Technology at Dhirubhai Ambani Institute of Information and Communication Technology and has not been submitted elsewhere for a degree,

ii) due acknowledgment has been made in the text to all the reference material used.

Kishankumar Vaishnani

Certificate

This is to certify that the thesis work entitled Deep Learning based Nuclei Segmentation in Histopathological Images: A perspective on Image Normalization has been carried out by Vaishnani Kishankumar Dineshkumar for the degree of Master of Technology in Information and Communication Technology at *Dhirubhai Ambani Institute of Information and Communication Technology* under our supervision.

Prof. Bakul Gohel
Thesis Supervisor

Prof. Avik Hati
Thesis Co-Supervisor

Acknowledgments

First and foremost, I would like to sincerely thank my supervisor, Prof. Bakul Sir, for his constant motivation, guidance, and support. Without his continuous help and trust, this thesis would not have been concluded. I am highly grateful for the insightful knowledge he has given to me.

I would also like to thank my co-guide, Prof. Avik Hati, who guided me whenever I faced challenges. He motivated me not to give up and work with consistency.

I want to thank Dr. Jignesh Vaishnani, who helped us identify the real-time problem faced in the hospital and labs.

Lastly, I would like to thank my parents, friends, and peers who have uplifted my morale at every step. It would have been a tedious journey without their constant motivation.

Contents

Abstract

Histopathology is the diagnosis and study of the different tissues. For diagnosis of different diseases, there are parameters like nuclei count, anatomy of nuclei, etc. However, identifying these parameters manually is a tedious and time-consuming task. Computer-aided diagnosis (CAD) helps smoothen the process. In CAD, nuclei segmentation is the crucial task of identifying the nuclei's anatomy that helps identify the diseases more efficiently. Many deep learning methodologies are present to do the task of nuclei segmentation, but all the methods work on the dataset provided at the time of training. However, there are high chances of the data variabilities present in Histopathology tissue slides due to the different scanners, variations in stain, storage conditions, etc. This kind of data variation affects the performance of any Deep Learning architecture. For that, color normalization techniques help to remove data variations between the histopathological images. So there are many techniques available to do the color normalization, but they have different reactions to the different datasets. So there is a problem with the selection of the normalization techniques. In this study, we have proposed a model that can help to use multiple normalization techniques simultaneously and feed them to the Deep Learning model to get a more robust architecture. We also performed cross data and self data analysis for the all viewed analysis.

List of Tables

List of Figures

CHAPTER 1
Introduction

Morphological changes in nuclei are essential to identify the many diseases [5] in histopathological images and give meaningful information to the clinic, specifically cancer [1]. Manual diagnosis of the disease is more time-consuming and tedious. Automated cell nuclei segmentation helps analyze cell nuclei, including counting of nuclei [22], cell type classification [12], etc. Hematoxylin and Eosin (H&E) stained histopathological image, and it's segmentation mask shown in Fig. 1.1

With rapid development in deep learning-based methods, Convolutional Neural networks have been dominant in the field of computer vision to do various tasks, including medical image segmentation [27] [26]. For example, In 2015, Ronnberg et al. proposed a Fully connected network (FCN) based UNET [18] to predict mask for brain dataset; C Hernandez proposed a featured pyramid network(FPN) combined with VGG to predict mask of the nuclei, Wang et al. [25] proposed a Mask RCNN model to handle small, dense nuclei in stains by incorporating a multi-path dilated residual network.

High variability in histopathological images makes deep learning-based methods less optimized to perform the segmentation task. High data variability occurs due to the concentration of the stain [3], storage condition of the slides [11], absorption of the light while converting into a digital image, different digitalization mediums, etc. And also, with this, there is a high variance in the morphology of the nuclei concerning the organ. To reduce these data variabilities, there are techniques like histogram equalization, spectral matching, color transfer, etc. But the histogram equalization Histogram matching methods are the method that will adjust the color in the RGB space through its respective image histogram, which will lead to the information loss [2]. Color transfer techniques find correspondences between segmented regions or dye channels [21]. The spectral matching techniques will normalize the image by each dye representation in RGB channels and dye concentrations in each image pixel. This technique will preserve the his-

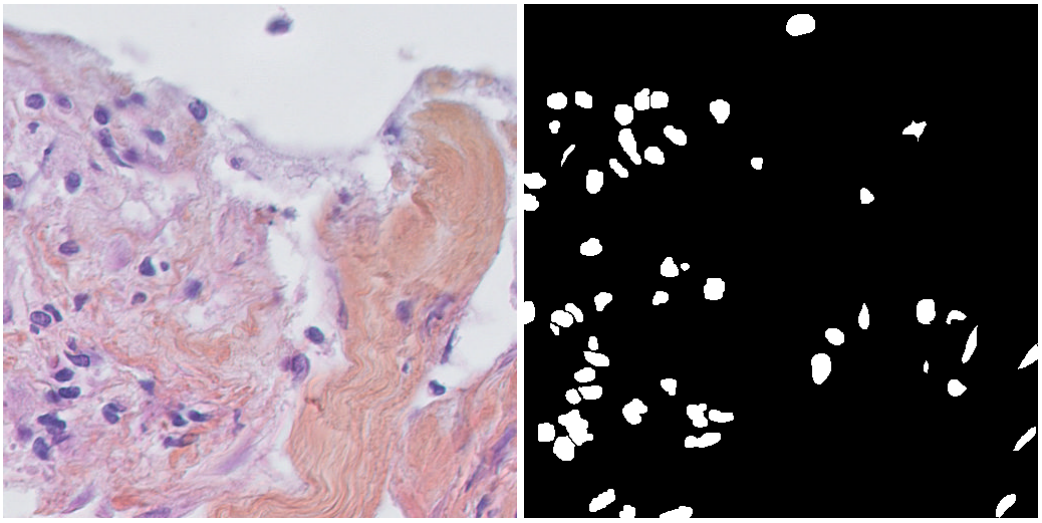

Figure 1.1: H&E stain image and it's Binary Mask

tological structure of the image. Macenko [13], Reinhard [17], and Vahadanne [23] all techniques are the maths-based techniques that will do color normalization of the histological image and preserve its histological structure and helps to reduce the color variations between the histopathological images.

The majority of the prior study used either single image augmentation [4] or single color normalization [20] technique in that method. In the present work, we evaluated which of these techniques showed better performance. We hypothesize the use of multiple normalization techniques may improve the performance; we have created many deep learning-based architectures. We also combine the multiple normalization methods simultaneously. These all techniques have different methods for applying color normalization to the histopathological image, but they have their own set of advantages to the image. So, in this study, we propose an architecture that can simultaneously use all the output of the data normalization techniques and enhance the segmentation result.

1.1 Our Contributions

In this study we are

- Studying the multiple color normalization techniques to reduce the data variabilities in a histopathological images.
- Proposing a nuclei segmentation architecture that is able to take the outputs of all the normalization techniques and raw image as a single input simultaneously.

- Performing cross data analysis using the MoNuSeg, CryoNuSeg and TNBC datasets.

1.2 Thesis Outline

This thesis is organised in 5 chapters

- Chapter 2 contains literature survey on data variabilities in histopathological image, Color normalization techniques and Deep Learning architecture for the nuclei segmentation
- Chapter 3 describes the multiple methodologies for the nuclei segmentation.
- Chapter 4 contains the implementation details, results of the experiments and related discussion.
- Chapter 5 concludes the thesis and defines scope of future work.

CHAPTER 2
Literature Review

In modern medicine, pathology is a critical field. Specifically, nuclei segmentation is an essential step in cancer analysis, diagnosis, and grading. Since these tests require high quality, it is of utmost importance that nuclei segmentation is performed with high accuracy. Traditionally, diagnostic and prognostic assessments are conducted by pathologists, but nowadays, with the advent of computerized methodologies, the need for human intervention has reduced. Many deep learning models have been proposed and taken over the traditional methods of nuclei segmentation.

2.1 Nuclei Segmentation

Deep convolutions networks have been employed extensively in order to detect and segment nuclei [7] Wang et al. [25] proposed a Mask RCNN model to handle small, dense nuclei in stains by incorporating a multi-path dilated residual network. They have cited that their model outperforms recognition and segmentation for small and dense targets. Hassan et al. [6] have employed FCDenseNets [9] for multi-center nuclei to combat the overlapped issues, clumped nuclei that may also have unclear boundaries. They trained each stain template individually using clustering followed by an aggregation operation to get a unified segmentation mask. They have outperformed state-of-art nuclei segmentation models due to their proposed algorithm.

Furthermore, Yang et al. [28] have also addressed the issue of overlapping nuclei and tried to resolve it by a deep learning architecture termed as Nuclear Segmentation Tool (NuSeT). This network combines two standard networks of Unet and Regional Proposal Network (RPN) over dataset consisting of 2D and 3D images. This hybrid model aids in reducing false positives and also addresses the issues such as variability in signal and shape, presence of artifacts, etc.

2.2 Data Variability

Deep Learning architectures perform well for the nuclei segmentation but are dataset dependent. So that if the dataset is of some type, if the dataset is changed, then the model will not be able to sustain. In histopathology, there are high chances of data variabilities due to factors like storage condition, digitalization medium, Concentration of stain, Absorption of light while converting into digital form, staining time, etc. Some of the affecting parameters are explained in brief in the following sections.

2.2.1 Staining

The stain is applied to the tissue to distinguish the cellular and histological components of the tissue. In this study, we have considered the H&E stain that will distinguish between nuclei and connectives. Various factors of the stain affect the color of the tissue-like stain time, pH of the solution [3] and concentration of the stain. Figure 2.1 illustrate the variance in color due to the stain.

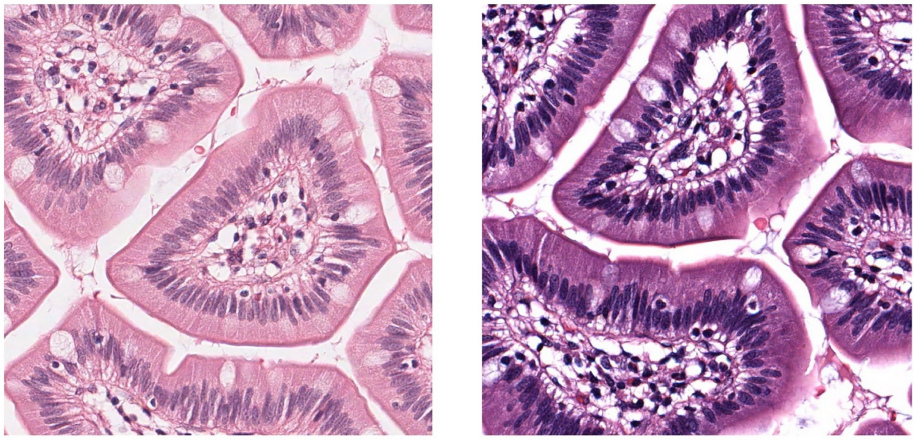

$\downarrow$H$\downarrow$E $\uparrow$H$\uparrow$E

Figure 2.1: Histological image with stain variation [8]

2.2.2 Digitization of the sample

When we try to convert the samples into the form digital, it shows the difference in the image; however, while using a different scanner, it also shows the variation in the histological image, which is shown in Figure 2.2

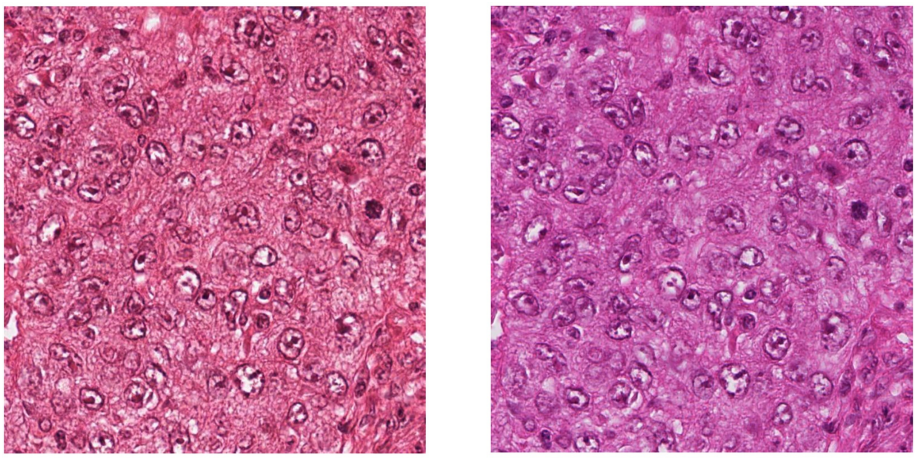

(a) (b)

Figure 2.2: Sample digitized by the Aperio XT (a) and Hamamatsu (b) [19]

2.2.3 Storage Condition

Another factor that affects the variation in the slide is how it is stored as stain interacts with the slide and also with the environmental condition, which causes its natural discoloration[11]. This variation in color due to this storage condition is shown in Figure 2.3.

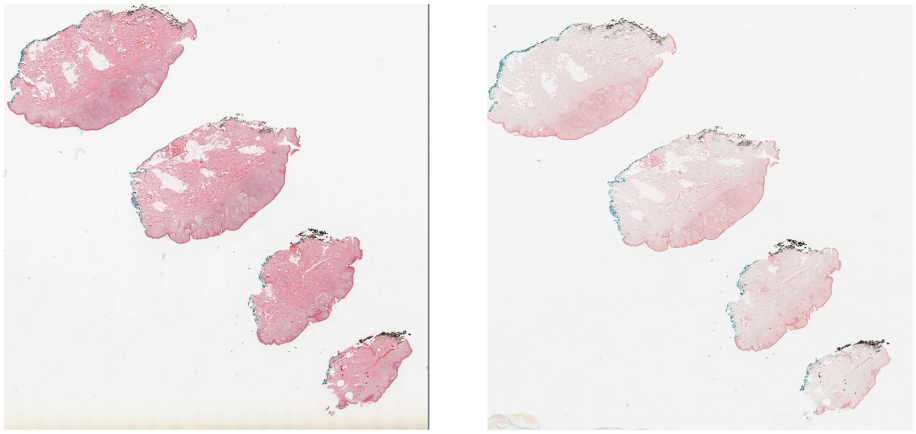

(a) (b)

Figure 2.3: Fading leads to color variation [24]

2.3 Data Normalization

Due to high data variance in the data, Data Normalization is highly impactable in the deep learning model. There are many data normalization techniques present that will reduce the impact of the variance on the model. These normalization

techniques classify into histogram matching, color transfer, and spectral matching. Histogram matching methods are the method that will adjust the color in the RGB space through its respective image histogram that will lead to the information loss [2]. Color transfer techniques either find correspondences between segmented regions or find correspondences between dyes channels [21]. The spectral matching techniques will normalize the image by each dye representation in RGB channels and dye concentrations in each image pixel. This technique will preserve the histological structure of the image.

Macenko [13], Reinhard [17], Vahadanne [23], all techniques are the maths based techniques that will do color normalization of the histological image and preserve its histological structure and helps to reduce the color variations between the histopathological images. From the following techniques, Reinhard and Vahadane are reference-based techniques, i.e., they will try to transfer all the histological images into provided reference image. Macenko is without reference-based technique, meaning that it will try to minimize the color variation by some static parameter of the stain.

2.3.1 Reinhard

The color transfer technique proposed by [17] aims at improving the image's color, which is deteriorated due to unwanted color cast. The color is corrected by borrowing the color characteristics from a target image of the required coloring. In RGB images, three channels are correlated; modification of one channel will require a subsequent change in another channel. This complicates manipulating an image for a target image. Hence, in this method the RGB images, both target I_t and source I_s are converted into a decorrelated $l\alpha\beta$ color space. l axis represents an achromatic channel,while the α and β channels are chromatic yellow–blue and red-green opponent channels.Equation (2.1) gives the equation for this conversion. Later these are converted to logarithmic values that ensure that uniform changes in channel intensities will be equally detected. The next step is the color correction. This is achieved by transferring the distribution of data points from the target image to the source image of these uncorrelated spaces. The source image data points are modified as given in Equation (2.2) and (2.3); essentially, here, the mean is removed from each channel, and then these values are scaled by the standard deviation of the target and source images. This methodology will transfer the look and feel of the target image to the source image. At last, the images are to be converted back to the RGB color space by Equation (2.4).

$$\begin{bmatrix} L \\ M \\ S \end{bmatrix} = \begin{bmatrix} 0.3897 & 0.6890 & -0.0787 \\ -0.2298 & 1.1834 & 0.0464 \\ 0.0000 & 0.0000 & 1.0000 \end{bmatrix} \begin{bmatrix} X \\ Y \\ Z \end{bmatrix} \tag{2.1}$$

$$\begin{aligned} l^* &= l - \langle l \rangle \\ \alpha^* &= \alpha - \langle \alpha \rangle \\ \beta^* &= \beta - \langle \beta \rangle \end{aligned} \tag{2.2}$$

$$\begin{aligned} l' &= \frac{\sigma_t^l}{\sigma_s^l} l^* \\ \alpha' &= \frac{\sigma_t^\alpha}{\sigma_s^\alpha} \alpha^* \\ \beta' &= \frac{\sigma_t^\beta}{\sigma_s^\beta} \beta^* \end{aligned} \tag{2.3}$$

$$\begin{bmatrix} R \\ G \\ B \end{bmatrix} = \begin{bmatrix} 4.4679 & -3.5873 & 0.1193 \\ -1.2186 & 2.3809 & -0.1624 \\ 0.0497 & -0.2439 & 1.2045 \end{bmatrix} \begin{bmatrix} L \\ M \\ S \end{bmatrix} \tag{2.4}$$

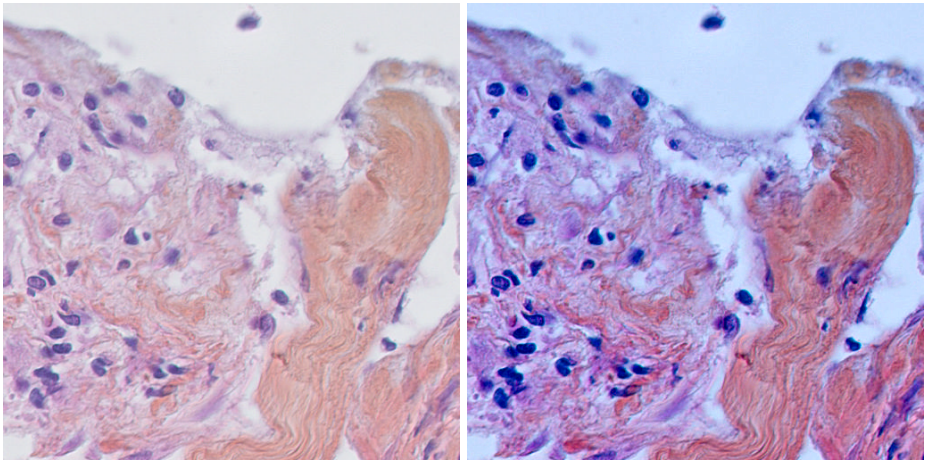

Figure 2.4: H&E stain image and Reinhard normalization technique applied image

2.3.2 Vahadane

Differences in raw materials and production procedures of stain vendors, staining protocols of labs, and color sensitivities of digital scanners all contribute to undesired color variations when staining and scanning tissue samples for microscopic analysis. Natural image techniques fail to use the structural features of stained

tissue samples, resulting in unwanted color distortions. We first decompose images in an unsupervised manner into sparse and non-negative stain density maps to simulate fundamental physical phenomena that define tissue structure. We integrate the stain density maps of a given image with the stain color base of a pathologist-preferred target image, changing just the image's color while keeping the structure provided by the maps. Compared to other methods, the correlation of stain density with ground truth and pathologist preference was higher for images normalized using our method. It consists mainly of three steps:

- Sparse Non-negative Matrix Factorization(SNMF) for Stain separation
- Structure Preserving Color Normalization
- Smart patch-based acceleration scheme for Whole Slide Image(WSI)

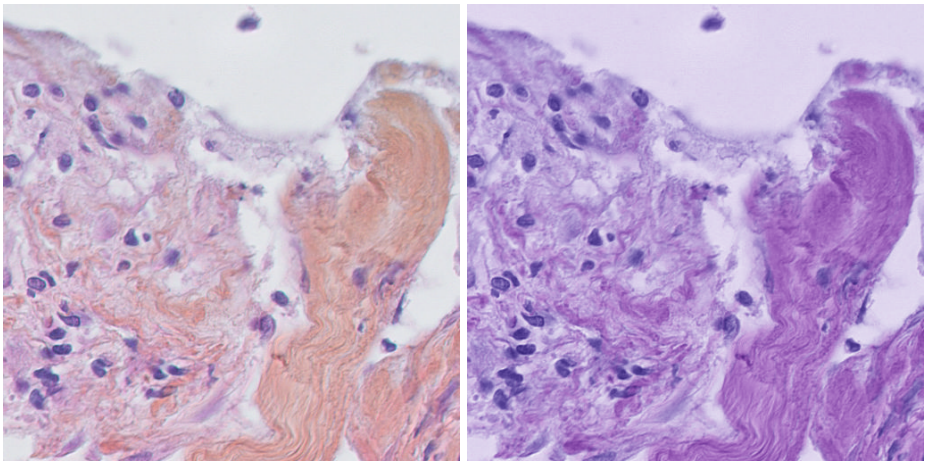

Figure 2.5: H&E stain image and Vahadane normalization technique applied image

2.3.3 Macenko without reference

This method helps overcome the inconsistencies in histology slide preparation's staining method. The stains absorb all the wavelengths of the input light's spectrum wherever it sticks firmly to the substance of the tissues. The proportion of each wavelength absorbed forms the stain vector. The stains vary primarily based on the quantity of stain added to the slide and how it was stored and handled after creation. To get optimal results, this technique normalizes multiple stains. The first step is to convert the color values of the stains, i.e., RGB vectors I, into their corresponding optical density (OD) values by following the Equation (2.5). Then the vectors with OD intensity less than 0.15 (threshold) are filtered out, and the

SVD of the rest of the stain vectors is calculated. Two vectors with the highest singular values are picked to form a plane. All of the stain vectors are projected onto these planes and are normalized to unit lengths. To map the directions of these vectors to a scalar value, the angle of each vector to the plane is calculated. Robust extremes from these angles are calculated and converted back to OD space. This represents the new optimal stain vector.

$$OD = -\log_{10}(I) \tag{2.5}$$

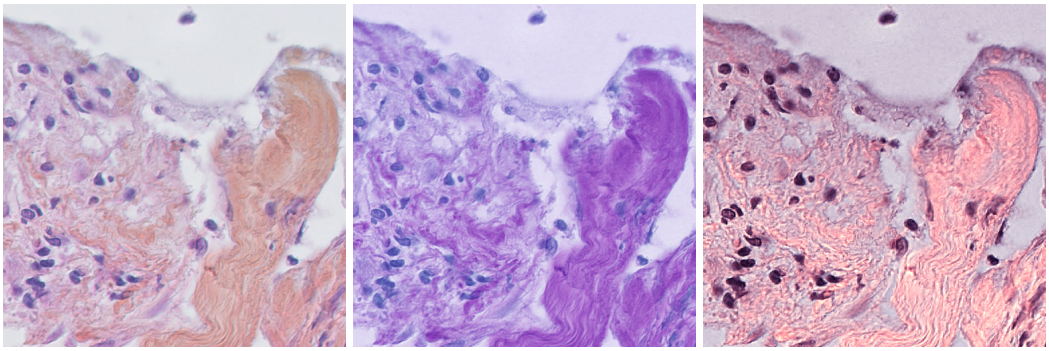

(a) (b) (c)

Figure 2.6: (a) H&E stain image, (b) Macenko with reference applied normalization technique and (c) Macenko without reference applied normalization technique

CHAPTER 3
Nuclei Segmentation Models

Nuclei segmentation is a semantic segmentation task where the motive is to localize the nuclei in the slice images. Pixel-wise classification is performed on the entire image to determine the pixels of nuclei. Convolution networks are prevalent in image segmentation tasks as they extract vital features from images. Moreover, Encoder-decoder architectures built using convolution networks, like UNET [18] perform excellently. The following subsections elaborate on the architectures we used in the proposed model.

3.1 UNET

In 2015 ronnaber [18] proposed UNET architecture for biomedical image segmentation. It is also considered an autoencoder architecture where the encoder will extract the semantic features from images. In contrast, the decoder will operate to upsample the features to generate the segmentation mask. This output mask can be of the same size or different sizes, allowing UNET architectures to perform denoizing, Super-resolution, and Segmentation on images.

One of the essential aspects of this architecture is the presence of skip connections between the encoder and the decoder part. They transfer spatial features to the decoder from the encoder, thereby helping in retaining the spatial information of the image. Additionally, the skip connections enable UNET to train faster and efficiently. We have used UNET architecture for the individual normalization technique's mask generation.

3.2 Multichannel UNET

The standard UNET does not take dynamic inputs and, therefore, can not handle multiple normalization techniques. Therefore, we have devised a multi-channel UNET by changing the number of channels at the input layer. For n number of

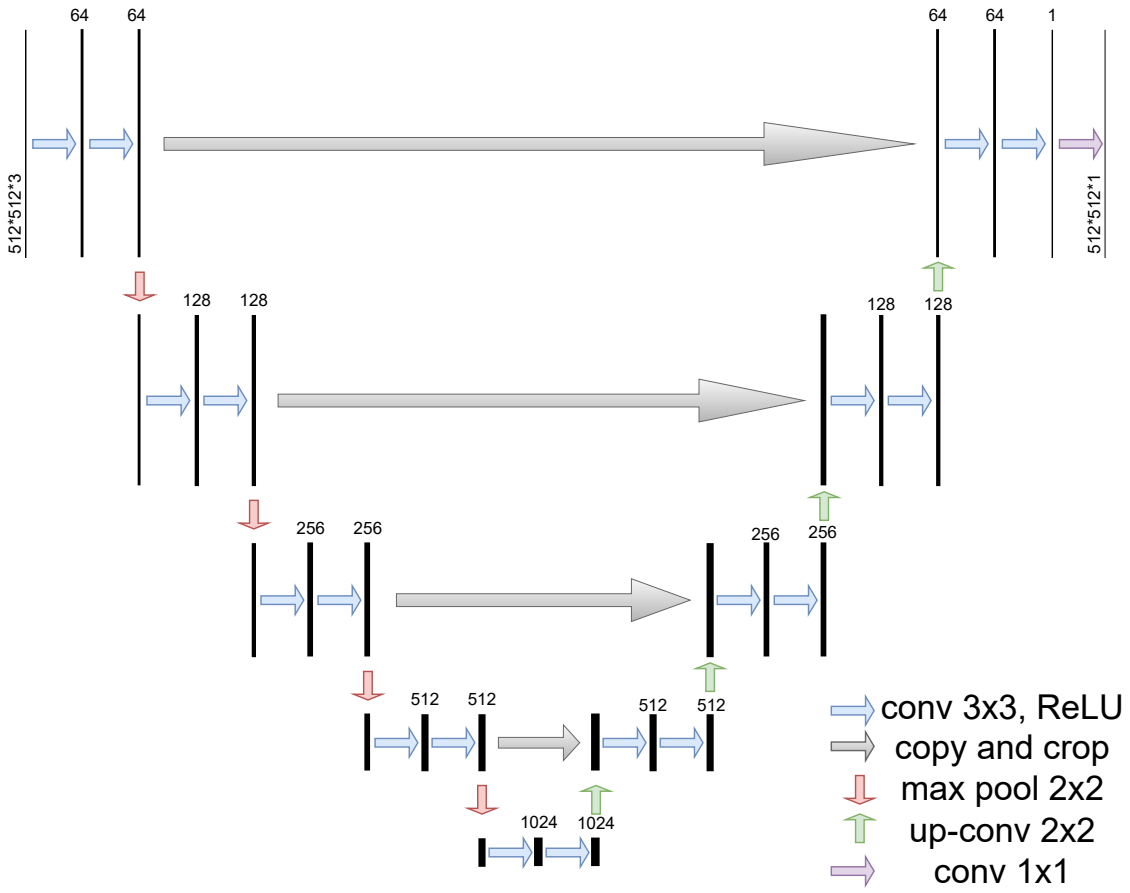

Figure 3.1: UNET Architecture

the normalization techniques, we will require n respective channels. Since we have RGB images with three color channels, they will require n channels for normalization. Hence, the input for n normalization will be 3n. Thus, here we have bypassed all the normalization techniques as a channel of the image. UNET yields the weight of each channel while generating the mask of the image, which in turn assigns weight to the respective normalization technique.

3.3 Parallel CNN

As we have a small nuclei size for the segmentation, due to the pooling layer, there are high chances of data loss of shape and size of the nuclei. In the following architecture, we have created five parallel CNN architectures. We extracted features from all five CNN, concatenated them, and applied them to the convolution layer. Skip connection is applied from the initial convolution layer before the output layer. Implementation of this architecture is shown in the Figure 3.4.

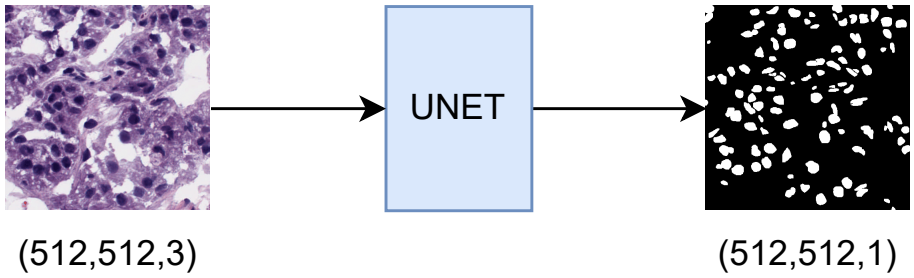

Figure 3.2: Pipeline for segmentation using UNET architecture considering input as either the raw image or output of one normalization technique

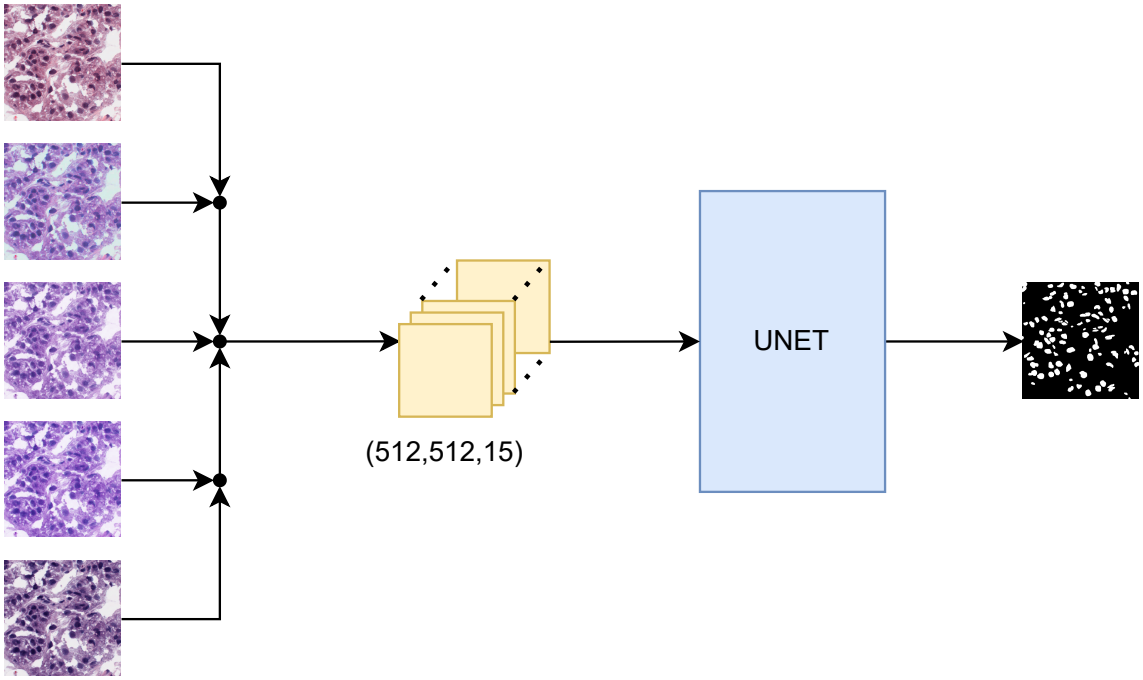

Figure 3.3: Pipeline for segmentation using UNET architecture considering input as combination of the raw image and the output of four normalization techniques

3.4 Parallel CNN with the Attention mechanism

The attention mechanism intuitively highlights the critical features of the input images. It is designed to allow the decoder to flexibly use the most relevant sections of the input sequence by combining all of the encoded input vectors into a weighted combination, with the most relevant vectors receiving the highest weights.

In 2019 Zhang et al. proposed Hierarchical second-order pooling (HSP) [29] based Deep Object Co-segmentation method that is used to get long-range dependency between the channels. The features from the encoders are passed to a convolution layer to reduce the number of channels for better computations. The

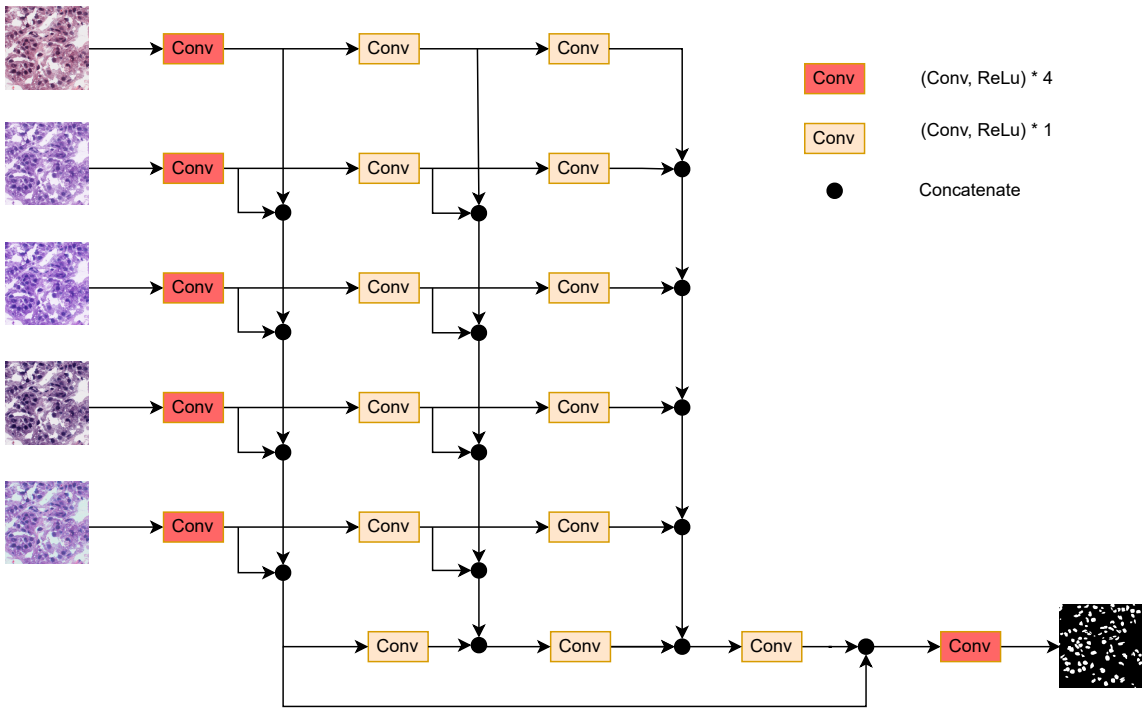

Figure 3.4: Pipeline for segmentation using parallel convolutional neural network architecture with fusion of features at different intermediate levels considering five input images: raw image and the output of four normalization techniques

feature maps taken from these layers are transferred to a pooling layer. This layer extracts the higher-order statistics from features. The resulting enhanced features from this channel modulator are concatenated for each image. These are again passed to this channel modulator to capture long-range dependency between the features to produce an activation value for each channel. This entire method is pictorially represented in Figure 3.6. We have combined this HSP with the UNET architecture. Five UNET architectures were created for the five different normalization techniques for the same input. The features were then extracted from the encoder and fed to the HSP module as shown in Figure 3.5 That HSP gives the five scalars that show the weightage of each normalization technique. And then, we perform the sum of the product of the HSP scalar with the five UNET outputs and get the final binary mask.

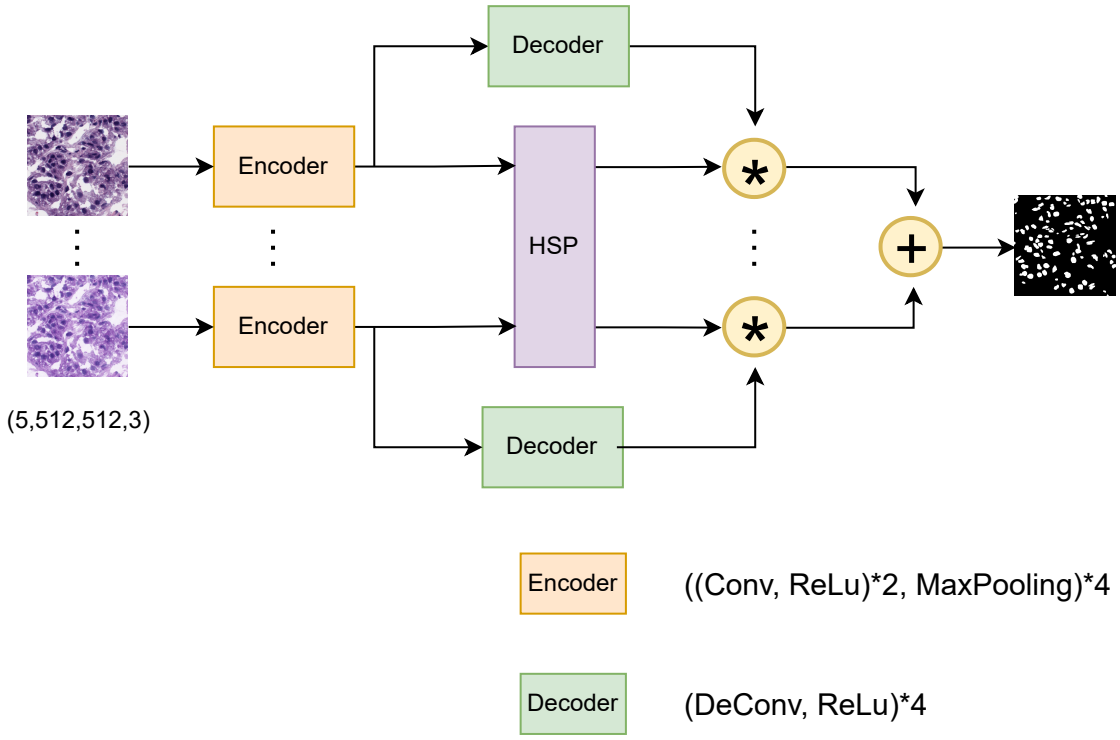

Figure 3.5: Pipeline for segmentation using attention based UNET architecture considering five input images: raw image and the output of four normalization techniques

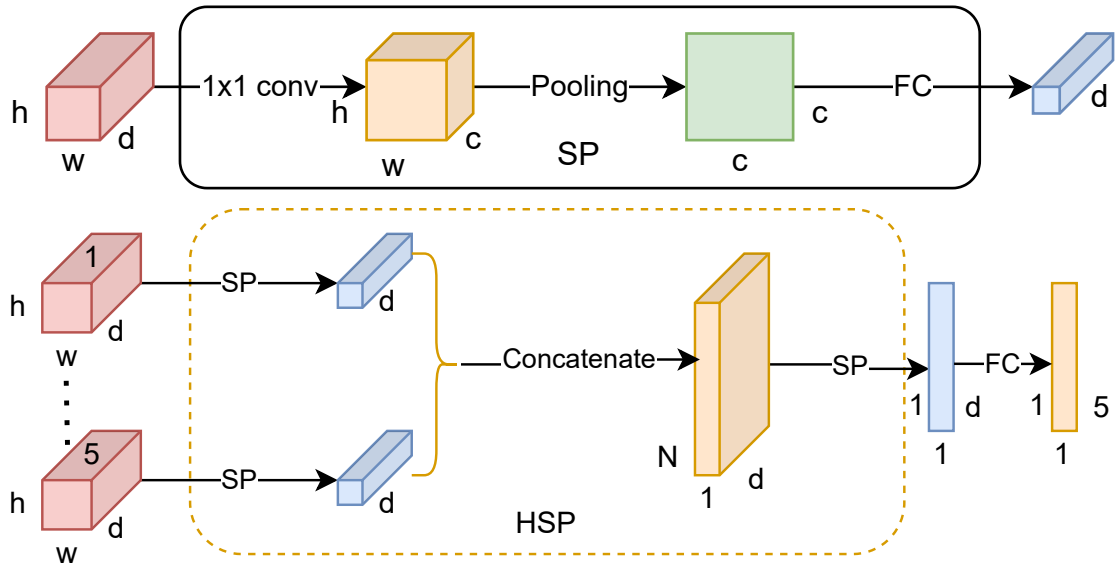

Figure 3.6: Spatial pooling (SP) and Hierarchical second-order pooling (HSP) Module

CHAPTER 4
Experiments

4.1 Implementation Details

For the experiments and results, standard UNET [18] architecture is used, but the number of filters used is 64, 128, 256, 512 for the encoder part and 512, 256, 128, 64 for the decoder part, respectively.

In this study, we have used the image size of 512×512. If the image size is less than this, then we have ignored it, and for large image size, we have used center cropping to make it 512×512. The Figures, 4.1 and 4.2 show the data distribution among each organ and count for each organ in the training and testing dataset of the MoNuSeg. Figure 4.3 shows the count of each organ in the CryoNuSeg whole (training and testing) dataset. TNBC dataset consists of only one Breast organ.

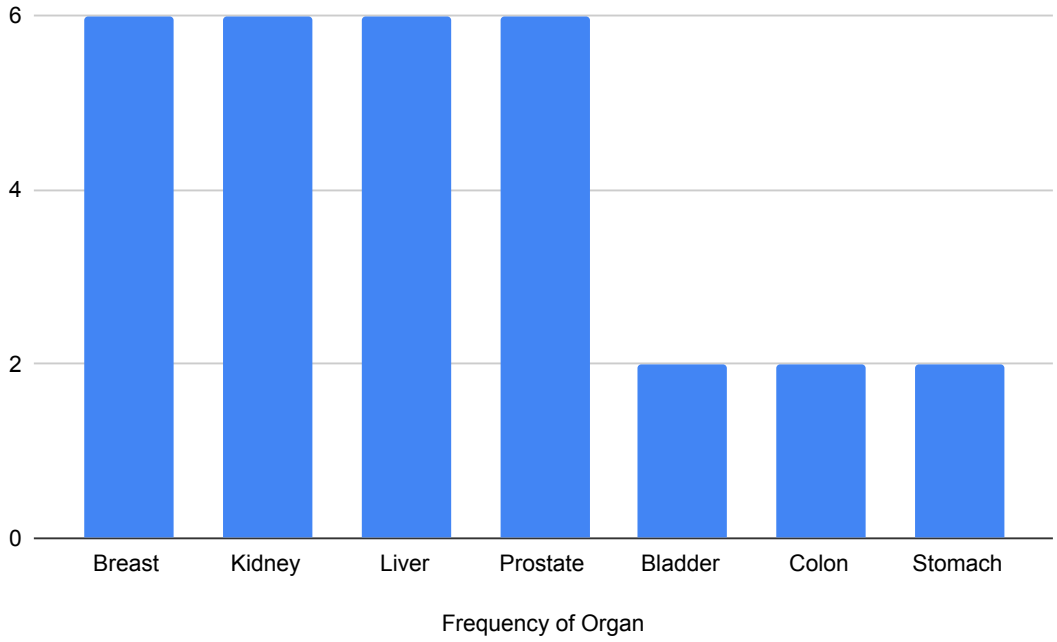

Figure 4.1: Count of each organ of MoNuSeg training dataset

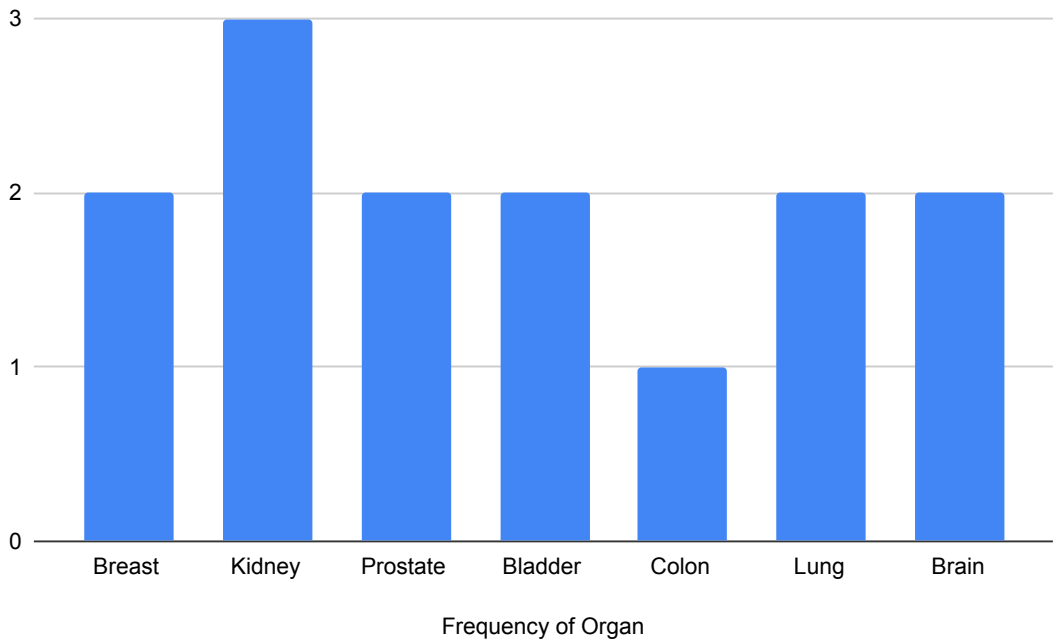

Figure 4.2: Count of each organ of MoNuSeg testing dataset

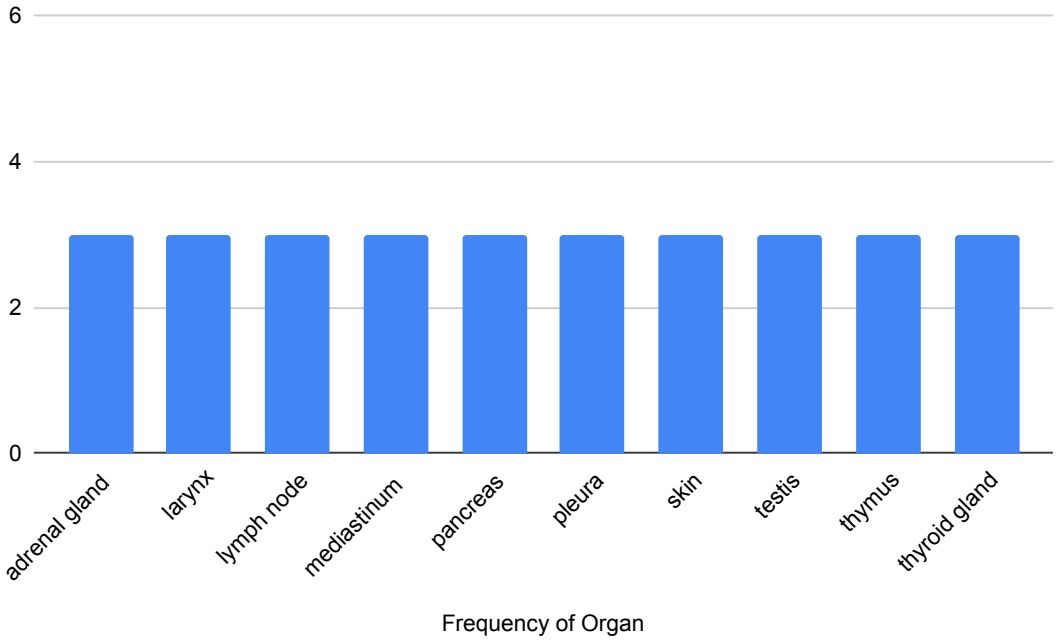

Figure 4.3: Count of each organ of CryoNuSeg whole (training and testing) dataset

4.2 Loss Function

Dice loss [15]was brought to the computer vision community by Milletari et al. in 2016 for 3D medical image segmentation for the unbalanced foreground and background. The nuclei segmentation task is highly unbalanced between the foreground nuclei and background. Use of the Binary cross Entropy [30] leads to trapped in the local minima of the loss function by predicting the more background part.

$$D = \frac{2\sum_i^N p_i g_i}{\sum_i^N p_i^2 + \sum_i^N g_i^2} \tag{4.1}$$

Where:
N = Number of pixels in a image
p_i = i^{th} pixel's class in a predicted image
g_i = i^{th} pixel's class in a ground truth image

4.3 Dataset

We have used a total of 3 datasets, namely Multi-Organ Nuclei Segmentation (MoNuSeg), Triple Negative Breast Cancer (TNBC), and CryoNuSeg. Summary of these dataset is present in a Table 4.1. In all the datasets, histopathological slides are acquired at 40x magnification and chosen from organs not present in the other publicly dataset. All the datasets are highly variable due to their distinct capture locations.

4.4 Performance Metrics

To measure the segmentation result in the form of a binary mask, the authors use Precision, Recall, F1-Score, and Relative error in Nuclei Count.

4.4.1 Precision

It is the ratio of correctly identified nuclei to the number of total detected nuclei.

$$\text{Precision}(P) = \frac{\text{True Positive}}{\text{True Positive} + \text{False Positive}} \tag{4.2}$$

Table 4.1: Dataset Descriptions

Dataset Name	**Image tiles**	**Tile size**	**Organs**	**Source**
MoNuSeg[10]	51	1000×1000	Breast Kidney Liver Prostate Bladder Colon Stomach Brain Lung	TCGA
CryoNuSeg[14]	30	512×512	adrenal gland larynx lymph node mediastinum pancreas pleura skin testis thymus thyroid gland	TCGA
TNBC[16]	50	512×512	Breast	Curie Inst.

4.4.2 Recall

The recall is the ratio of correctly identified nuclei to the number of nuclei present in the ground truth image.

$$\text{Recall}(R) = \frac{\text{True Positive}}{\text{True Positive} + \text{False Negative}} \tag{4.3}$$

4.4.3 F1 Score

F1 score is the harmonic mean of the Precision and Recall, which is best to judge the classifier over the precision & recall trade-off.

$$\text{F1 Score}(F) = 2 * \frac{\text{Precision} * \text{Recall}}{\text{Precision} + \text{Recall}} \tag{4.4}$$

4.4.4 Relative error in Nuclei Count

To count the nuclei, calculate the number of the connected region in the binary mask. The absolute difference in the nuclei count to the actual count is considered the relative error in the nuclei count.

$$\text{Relative Error in Nuclei Count}(E) = \frac{|\text{Ground Truth Count} - \text{Predicted Count}|}{\text{Ground Truth Count}} \tag{4.5}$$

4.5 Results

For the analytical purpose, we have performed self data and cross-data analyses. MoNuSeg has its test dataset to evaluate the model for the data analysis. Moreover, for the CryoNuSeg and TNBC, we split the dataset into 70:30 for training and testing purposes. Self-data analysis means if the training dataset is A's training part, then the testing dataset is also A's testing part. Cross-Data analysis means if the training dataset is A's training part, then the testing dataset will be B's whole (training and testing) dataset. In the study, we have performed both cross and self data analysis for all the three datasets: CryoNuSeg, MoNuSeg, and TNBC mentioned in the Table 4.1.

4.5.1 Quantitative Results

The table 4.2 represents the result of the UNET is trained using MoNuSeg training data and tested using the MoNuSeg, CryoNuSeg, and TNBC. Testing dataset MoNuSeg represents the self data analysis. Testing dataset CryoNuSeg and TNBC represent cross-data analysis. Here we measure the Precision, Recall, F1 Score, and Percentage Error in Count for the images. We have calculated each image's performance measures individually and then calculated the average and standard deviation for evaluation. Other tables Table 4.3 and Table 4.4 also form in the similar format and training using the UNET architecture.

Following tables table 4.5 and table 4.6 and 4.7 are result of the UNET Multichannel architecture. All these three tables performed self and cross data analysis.

Table 4.2: Quantitative results of Segmentation obtained using UNET architecture 3.1. Training is performed on the MoNuSeg dataset and the testing is performed on MoNuSeg dataset (self data analysis), and on CryoNuSeg and TNBC datasets (cross data analysis). Raw image and output of four normalization techniques (Macenko, Macenko without refernce (Macenko_wr) [13], Vahadane [23], Reinhard [17]) are used as the input.

Training Dataset: MoNuSeg		Testing Dataset		
Performance Metrics	Normalization Method	TNBC	CryoNuSeg	MoNuSeg
Precision (P)	Images	**0.89 ±0.09**	0.63 ±0.17	0.71 ±0.07
	Macenko	0.43 ±0.25	0.65 ±0.16	0.72 ±0.06
	Macenko_wr	0.75 ±0.23	**0.75 ±0.15**	**0.84 ±0.04**
	Vanhadane	0.52 ±0.24	0.67 ±0.15	0.75 ±0.05
	Reinhard	0.52 ±0.23	0.63 ±0.17	0.64 ±0.09
Recall (R)	Images	0.43 ±0.21	**0.90 ±0.05**	0.87 ±0.07
	Macenko	**0.90 ±0.06**	0.87 ±0.04	0.85 ±0.05
	Macenko_wr	0.66 ±0.15	0.79 ±0.06	0.74 ±0.09
	Vanhadane	0.86 ±0.07	0.86 ±0.04	0.83 ±0.06
	Reinhard	0.84 ±0.06	0.87 ±0.07	**0.89 ±0.06**
F1 Score (F)	Images	0.54 ±0.20	0.72 ±0.10	0.78 ±0.04
	Macenko	0.53 ±0.25	0.73 ±0.10	0.78 ±0.03
	Macenko_wr	**0.66 ±0.17**	**0.76 ±0.08**	0.78 ±0.05
	Vanhadane	0.60 ±0.23	0.74 ±0.10	**0.78 ±0.03**
	Reinhard	0.60 ±0.23	0.71 ±0.11	0.74 ±0.07
Error in Count (E)	Images	**0.35 ±0.20**	0.26 ±0.19	0.10 ±0.11
	Macenko	0.56 ±0.97	0.29 ±0.20	0.10 ±0.07
	Macenko_wr	1.10 ±4.05	**0.23 ±0.12**	0.07 ±0.05
	Vanhadane	1.05 ±2.44	0.24 ±0.17	**0.07 ±0.04**
	Reinhard	0.93 ±1.95	0.24 ±0.16	0.11 ±0.09

4.5.2 Qualitative Results

Figure 4.4 shows the visual output of the methodologies described in the result section. This result shows that Multichannel's performance is comparable to the Reinhard normalization applied UNET trained model.

Figure 4.5 shows the visual output of the methodology described in the result section. This result shows that Reinhard performs better than all the other UNET architecture-trained models using single input of the normalization techniques.

Table 4.3: Quantitative results of Segmentation obtained using UNET architecture 3.1. Training is performed on the CryoNuSeg dataset and the testing is performed on CryoNuSeg dataset (self data analysis), and on TNBC and MoNuSeg datasets (cross data analysis). Raw image and output of four normalization techniques (Macenko, Macenko without refernce (Macenko_wr) [13], Vahadane [23], Reinhard [17]) are used as the input.

Training Dataset: CryoNuSeg		Testing Dataset		
Performance Measure	Normalization Method	TNBC	CryoNuSeg	MoNuSeg
Precision (P)	Images	**0.95±0.04**	0.71±0.15	0.79±0.09
	Macenko	0.75±0.22	**0.83±0.11**	**0.84±0.06**
	Macenko_wr	0.81±0.22	0.77±0.13	0.82±0.06
	Vanhadane	0.73±0.18	0.77±0.13	0.80±0.06
	Reinhard	0.50±0.24	0.71±0.14	0.75±0.07
Recall (R)	Images	0.09±0.10	0.80±0.22	0.58±0.35
	Macenko	0.42±0.24	0.61±0.13	0.50±0.22
	Macenko_wr	0.29±0.24	0.74±0.10	0.55±0.27
	Vanhadane	0.52±0.23	0.73±0.08	0.59±0.22
	Reinhard	**0.78±0.19**	**0.85±0.07**	**0.73±0.16**
F1 Score (F)	Images	0.17±0.14	0.71±0.15	0.59±0.29
	Macenko	0.46±0.22	0.69±0.09	0.59±0.20
	Macenko_wr	0.34±0.22	0.74±0.06	0.61±0.24
	Vanhadane	0.55±0.16	0.74±0.07	0.65±0.17
	Reinhard	**0.55±0.19**	**0.76±0.08**	**0.73±0.10**
Error in Count (E)	Images	0.80±0.17	0.26±0.22	0.34±0.31
	Macenko	**0.61±0.88**	0.15±0.10	0.16±0.14
	Macenko_wr	0.81±0.92	**0.13±0.10**	0.21±0.24
	Vanhadane	0.72±2.17	0.18±0.13	**0.14±0.13**
	Reinhard	1.6±4.02	0.24±0.17	0.18±0.22

4.6 Discussion

We observed that the trained model with the color normalization technique works better than the model trained on only raw images. Without color normalized techniques, the image may give a good result on the self dataset, but the color normalization techniques perform well on the cross-data analysis. We have done training in UNET architecture for each normalization method's output for each dataset. Then we observed that Vahadane and Reinhard performed well overall. Still, cross-data analysis Reinhard performs well when it's come to the overall performance concerning the minor variance. For the architecture like simultaneously applying the output of each normalization technique, i.e., Multichannel UNET, UNET with attention mechanism, Parallel CNN; Multichannel UNET performed

Table 4.4: Quantitative results of Segmentation obtained using UNET architecture 3.1. Training is performed on the TNBC dataset and the testing is performed on TNBC dataset (self data analysis), and on CryoNuSeg and MoNuSeg datasets (cross data analysis). Raw image and output of four normalization techniques (Macenko, Macenko without refernce (Macenko_wr) [13], Vahadane [23], Reinhard [17]) are used as the input.

Training Dataset: TNBC		Testing Dataset		
Performance Measure	Normalization Method	TNBC	CryoNuSeg	MoNuSeg
Precision (P)	Images	0.75 ±0.10	0.55 ±0.17	0.67 ±0.16
	Macenko	0.74 ±0.21	0.78 ±0.12	0.82 ±0.07
	Macenko_wr	0.76 ±0.21	**0.80 ±0.10**	**0.83 ±0.07**
	Vanhadane	0.74 ±0.21	0.77 ±0.13	0.82 ±0.06
	Reinhard	**0.76 ±0.09**	0.67 ±0.15	0.74 ±0.08
Recall (R)	Images	**0.85 ±0.07**	**0.93 ±0.06**	0.79 ±0.26
	Macenko	0.79 ±0.09	0.65 ±0.10	0.68 ±0.13
	Macenko_wr	0.76 ±0.11	0.54 ±0.15	0.61 ±0.18
	Vanhadane	0.77 ±0.11	0.67 ±0.11	0.69 ±0.12
	Reinhard	0.79 ±0.10	0.74 ±0.10	**0.79 ±0.09**
F1 Score (F)	Images	**0.79 ±0.06**	0.67 ±0.13	0.66 ±0.17
	Macenko	0.73 ±0.19	0.70 ±0.08	0.74 ±0.08
	Macenko_wr	0.73 ±0.21	0.63 ±0.12	0.68 ±0.12
	Vanhadane	0.73 ±0.19	**0.70 ±0.08**	0.74 ±0.08
	Reinhard	0.77 ±0.06	0.69 ±0.09	**0.76 ±0.05**
Error in Count (E)	Images	**0.25 ±0.27**	0.40 ±0.21	0.33 ±0.33
	Macenko	1.03 ±2.95	**0.24 ±0.13**	0.33 ±0.33
	Macenko_wr	0.46 ±0.90	0.42 ±0.14	0.28 ±0.15
	Vanhadane	0.93 ±2.61	0.27 ±0.14	0.17 ±0.13
	Reinhard	0.31 ±0.44	0.24 ±0.17	**0.16 ±0.16**

better than all. It means if we provide the additional feature while providing input, that will give you better results as all the encoder and decoder parts can use all the features. While comparing UNET trained on a single normalization technique's output with the multichannel UNET, multichannel UNET gives a comparable result to the Reinhard normalization techniques. Nuclei count is also one of the applications of the Nuclei Segmentation. So as we observed that relative error in nuclei count is directly proportional to the Precision. We have selected the datasets with single tissue and Multi tissue and trained the UNET and multichannel UNET architecture with all the datasets. Then while performing cross-data analysis, we have observed that UNET architecture trained on the single dataset does not outperform for that specific tissue while performing cross-data analysis of a multi-tissue dataset.

Table 4.5: Quantitative results of Segmentation obtained using Multichannel UNET architecture 3.2. Training is performed on the TNBC dataset and the testing is performed on TNBC dataset (self data analysis), and on CryoNuSeg and MoNuSeg datasets (cross data analysis). Raw image and output of four normalization techniques (Macenko, Macenko without refernce (Macenko_wr) [13], Vahadane [23], Reinhard [17]) are used as the input.

Training Datset: TNBC	Testing Dataset		
Performance Measure	TNBC	CryoNuSeg	MoNuSeg
Precision (P)	0.73 $\pm$0.20	0.51 $\pm$0.17	0.59 $\pm$0.13
Recall (R)	0.79 $\pm$0.12	0.94 $\pm$0.03	0.92 $\pm$0.08
F1 Score (F)	0.74 $\pm$0.18	0.64 $\pm$0.14	0.70 $\pm$0.09
Error in Count (E)	0.51 $\pm$0.99	0.60 $\pm$0.23	0.37 $\pm$0.29

Table 4.6: Quantitative results of Segmentation obtained using Multichannel UNET architecture 3.2. Training is performed on the MoNuSeg dataset and the testing is performed on MoNuSeg dataset (self data analysis), and on CryoNuSeg and TNBC datasets (cross data analysis). Raw image and output of four normalization techniques (Macenko, Macenko without refernce (Macenko_wr) [13], Vahadane [23], Reinhard [17]) are used as the input.

Training Datset: MoNuSeg	Testing Dataset		
Performance Measure	TNBC	CryoNuSeg	MoNuSeg
Precision (P)	0.88 $\pm$0.15	0.68 $\pm$0.16	0.75 $\pm$0.09
Recall (R)	0.35 $\pm$0.17	0.83 $\pm$0.08	0.79 $\pm$0.12
F1 Score (F)	0.46 $\pm$0.17	0.73 $\pm$0.10	0.76 $\pm$0.05
Error in Count (E)	0.48 $\pm$0.31	0.27 $\pm$0.18	0.13 $\pm$0.08

Table 4.7: Quantitative results of Segmentation obtained using Multichannel UNET architecture 3.2. Training is performed on the CryoNuSeg dataset and the testing is performed on CryoNuSeg dataset (self data analysis), and on TNBC and MoNuSeg datasets (cross data analysis). Raw image and output of four normalization techniques (Macenko, Macenko without refernce (Macenko_wr) [13], Vahadane [23], Reinhard [17]) are used as the input.

Training Datset: CryoNuSeg	Testing Dataset		
Performance Measure	TNBC	CryoNuSeg	MoNuSeg
Precision (P)	0.96 $\pm$0.09	0.81 $\pm$0.12	0.83 $\pm$0.07
Recall (R)	0.04 $\pm$0.08	0.66 $\pm$0.18	0.50 $\pm$0.29
F1 Score (F)	0.08 $\pm$0.12	0.70 $\pm$0.15	0.56 $\pm$0.26
Error in Count (E)	0.89 $\pm$0.15	0.20 $\pm$0.18	0.26 $\pm$0.27

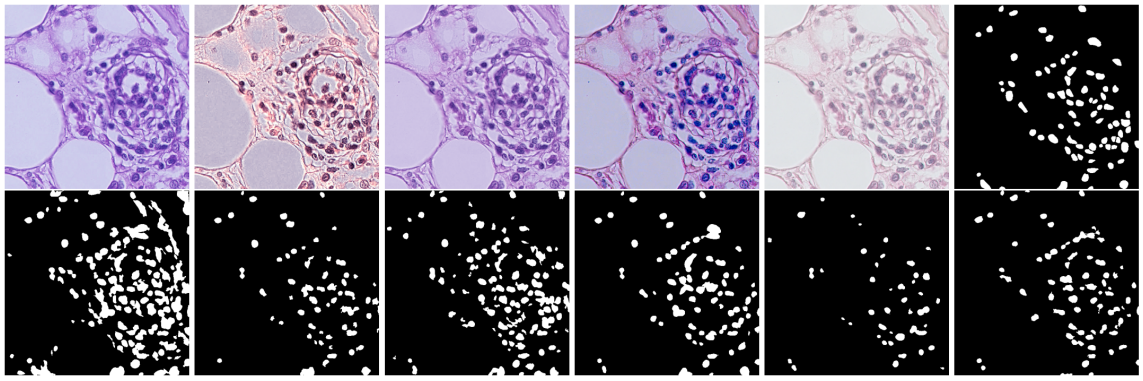

Prediction Macenko	Prediction Macenko_wr	Prediction Vahadane	Prediction Reinhard	Prediction Raw Image	Prediction MultiChannel
P=0.81	P=0.37	P=0.74	P=0.53	P=0.72	P=0.70
R=0.30	R=0.84	R=0.49	R=0.71	R=0.72	R=0.54
F=0.44	F=0.52	F=0.59	F=0.60	F=0.72	F=0.61
E=0.45	E=0.35	E=0.22	E=0.30	E=0.14	E=0.12

Figure 4.4: Visual results one of segmentation using UNET architecture considering input as the raw image and output of different normalization techniques separately and jointly (Multichannel); P=Precision, R=Recall, F=F1 Score, E=Error in nuclei count

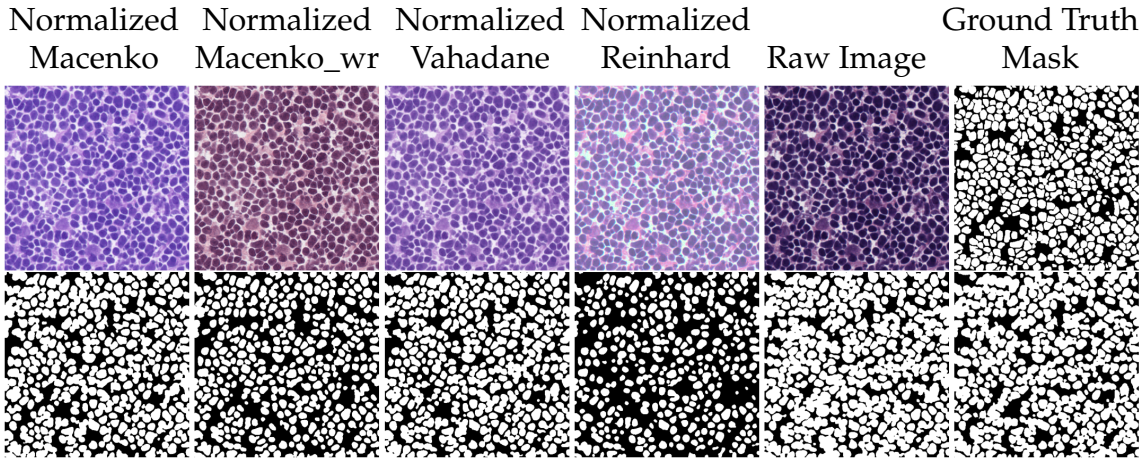

Prediction Macenko	Prediction Macenko_wr	Prediction Vahadane	Prediction Reinhard	Prediction Raw Image	Prediction MultiChannel
P=0.81	P=0.86	P=0.92	P=0.87	P=0.95	P=0.83
R=0.92	R=0.87	R=0.76	R=0.85	R=0.62	R=0.89
F=0.86	F=0.86	F=0.83	F=0.86	F=0.75	F=0.86
E=0.72	E=0.53	E=0.19	E=0.43	E=0.19	E=0.74

Figure 4.5: Visual results two of segmentation using UNET architecture considering input as the raw image and output of different normalization techniques separately and jointly (Multichannel); P=Precision, R=Recall, F=F1 Score, E=Error in nuclei count

CHAPTER 5
Conclusion and Future Work

In this work, we have analyzed the four normalization techniques and trained UNET architecture with the Raw image and output of the four normalization techniques to do segmentation of the nuclei. All the normalization techniques performed well compared to the Raw image, but Reinhard performed well among all the normalization techniques, including cross-data analysis. But the training of the UNET 3.1 architecture with the output of the single normalization techniques fails for some images due to some mathematical constraint or gives NA as a segmentation mask. This kind of failure has not occurred for the proposed multichannel UNET 3.2 architecture. Multichannel UNET architecture is comparable to UNET architecture trained with the output of the Reinhard normalization technique. For more unexpected dataset we recommend to use of multichannel UNET to overcome the failure.

We have done cross dataset analysis with a limited number of the organs. One can perform a more tissue-specific analysis that can help to see the morphology of the nuclei and helps to make a better and more generalized segmentation model. Only three normalization techniques have been explored in this study to make a generalized model. Still, there are many more advanced image processing and deep learning-based normalization techniques that can explore. This summons the future work of this thesis.

References

[1] T. Aoki, A. Yamada, Y. Kato, H. Saito, A. Tsuboi, A. Nakada, R. Niikura, M. Fujishiro, S. Oka, S. Ishihara, et al. Automatic detection of various abnormalities in capsule endoscopy videos by a deep learning-based system: a multicenter study. *Gastrointestinal Endoscopy*, 93(1):165–173, 2021.

[2] M. Beena et al. A survey on color normalization approach to histopathology images. *International Journal of Advanced Engineering Research and Science*, 3(4):103–105, 2016.

[3] C. C. Bilgin, J. Rittscher, R. Filkins, and A. Can. Digitally adjusting chromogenic dye proportions in brightfield microscopy images. *Journal of microscopy*, 245(3):319–330, 2012.

[4] Z. Eaton-Rosen, F. Bragman, S. Ourselin, and M. J. Cardoso. Improving data augmentation for medical image segmentation. 2018.

[5] V. Gulshan, L. Peng, M. Coram, M. C. Stumpe, D. Wu, A. Narayanaswamy, S. Venugopalan, K. Widner, T. Madams, J. Cuadros, et al. Development and validation of a deep learning algorithm for detection of diabetic retinopathy in retinal fundus photographs. *Jama*, 316(22):2402–2410, 2016.

[6] L. Hassan, M. Abdel-Nasser, A. Saleh, O. A. Omer, and D. Puig. Efficient stain-aware nuclei segmentation deep learning framework for multi-center histopathological images. *Electronics*, 10(8), 2021.

[7] H. Irshad, A. Veillard, L. Roux, and D. Racoceanu. Methods for nuclei detection, segmentation and classification in digital histopathology: A review current status and future potential. *IEEE reviews in biomedical engineering*, 7:97–114, 05 2014.

[8] A. Janowczyk, A. Basavanhally, and A. Madabhushi. Stain normalization using sparse autoencoders (stanosa): application to digital pathology. *Computerized Medical Imaging and Graphics*, 57:50–61, 2017.

[9] S. Jégou, M. Drozdzal, D. Vázquez, A. Romero, and Y. Bengio. The one hundred layers tiramisu: Fully convolutional densenets for semantic segmentation. *CoRR*, abs/1611.09326, 2016.

[10] N. Kumar, R. Verma, S. Sharma, S. Bhargava, A. Vahadane, and A. Sethi. A dataset and a technique for generalized nuclear segmentation for computational pathology. *IEEE transactions on medical imaging*, 36(7):1550–1560, 2017.

[11] X. Li and K. N. Plataniotis. A complete color normalization approach to histopathology images using color cues computed from saturation-weighted statistics. *IEEE Transactions on Biomedical Engineering*, 62(7):1862–1873, 2015.

[12] Y. Liu and F. Long. Acute lymphoblastic leukemia cells image analysis with deep bagging ensemble learning. In *ISBI 2019 C-NMC Challenge: Classification in Cancer Cell Imaging*, pages 113–121. Springer, 2019.

[13] M. Macenko, M. Niethammer, J. S. Marron, D. Borland, J. T. Woosley, X. Guan, C. Schmitt, and N. E. Thomas. A method for normalizing histology slides for quantitative analysis. In *2009 IEEE International Symposium on Biomedical Imaging: From Nano to Macro*, pages 1107–1110, 2009.

[14] A. Mahbod, G. Schaefer, B. Bancher, C. Löw, G. Dorffner, R. Ecker, and I. Ellinger. Cryonuseg: A dataset for nuclei instance segmentation of cryosectioned h&e-stained histological images. *Computers in Biology and Medicine*, 132:104349, 2021.

[15] F. Milletari, N. Navab, and S.-A. Ahmadi. V-net: Fully convolutional neural networks for volumetric medical image segmentation. In *IEEE Fourth International Conference on 3D Vision (3DV)*, pages 565–571, 2016.

[16] R. Raju, A. M. Paul, V. Asokachandran, B. George, L. Radhamony, M. Vinaykumar, R. Girijadevi, and M. R. Pillai. The triple-negative breast cancer database: an omics platform for reference, integration and analysis of triple-negative breast cancer data. *Breast Cancer Research*, 16(6):1–3, 2014.

[17] E. Reinhard, M. Adhikhmin, B. Gooch, and P. Shirley. Color transfer between images. *IEEE Computer graphics and applications*, 21(5):34–41, 2001.

[18] O. Ronneberger, P. Fischer, and T. Brox. U-net: Convolutional networks for biomedical image segmentation. In *Springer International Conference on Medical image computing and computer-assisted intervention*, pages 234–241, 2015.

[19] L. Roux, D. Racoceanu, N. Loménie, M. Kulikova, H. Irshad, J. Klossa, F. Capron, C. Genestie, G. Le Naour, and M. N. Gurcan. Mitosis detection in breast cancer histological images an icpr 2012 contest. *Journal of Pathology Informatics*, 4:34–42, 2013.

[20] S. Roy, A. kumar Jain, S. Lal, and J. Kini. A study about color normalization methods for histopathology images. *Micron*, 114:42–61, 2018.

[21] T. A. A. Tosta, P. R. de Faria, L. A. Neves, and M. Z. do Nascimento. Computational normalization of h&e-stained histological images: Progress, challenges and future potential. *Artificial Intelligence in Medicine*, 95:118–132, 2019.

[22] T. Tran, O.-H. Kwon, K.-R. Kwon, S.-H. Lee, and K.-W. Kang. Blood cell images segmentation using deep learning semantic segmentation. In *2018 IEEE International Conference on Electronics and Communication Engineering (ICECE)*, pages 13–16, 2018.

[23] A. Vahadane, T. Peng, A. Sethi, S. Albarqouni, L. Wang, M. Baust, K. Steiger, A. M. Schlitter, I. Esposito, and N. Navab. Structure-preserving color normalization and sparse stain separation for histological images. *IEEE transactions on medical imaging*, 35(8):1962–1971, 2016.

[24] J. Vicory, H. D. Couture, N. E. Thomas, D. Borland, J. Marron, J. Woosley, and M. Niethammer. Appearance normalization of histology slides. *Computerized Medical Imaging and Graphics*, 43:89–98, 2015.

[25] E. K. Wang, X. Zhang, L. Pan, C. Cheng, A. Dimitrakopoulou-Strauss, Y. Li, and N. Zhe. Multi-path dilated residual network for nuclei segmentation and detection. *Cells*, 8(5):499, May 2019. 31126166[pmid].

[26] Y. Xu, Z. Jia, L.-B. Wang, Y. Ai, F. Zhang, M. Lai, I. Eric, and C. Chang. Large scale tissue histopathology image classification, segmentation, and visualization via deep convolutional activation features. *BMC bioinformatics*, 18(1):1–17, 2017.

[27] S. S. Yadav and S. M. Jadhav. Deep convolutional neural network based medical image classification for disease diagnosis. *Journal of Big Data*, 6(1):1–18, 2019.

[28] L. Yang, R. Ghosh, J. Franklin, S. Chen, C. You, R. Narayan, M. Melcher, and J. Liphardt. Nuset: A deep learning tool for reliably separating and analyzing crowded cells. *PLoS computational biology*, 16:e1008193, 09 2020.

[29] K. Zhang, J. Chen, B. Liu, and Q. Liu. Deep object co-segmentation via spatial-semantic network modulation. In *Proceedings of the AAAI Conference on Artificial Intelligence*, volume 34, pages 12813–12820, 2020.

[30] Z. Zhang and M. Sabuncu. Generalized cross entropy loss for training deep neural networks with noisy labels. *Advances in Nural Information Processing Systems*, 31:112–123, 2018.